Available online at www.sciencedirect.com
SCIENCE DIRECT®
Journal of Catalysis 233 (2005) 221–233
JOURNAL OF CATALYSIS
www.elsevier.com/locate/jcat

# Direct conversion of methane to methyl acetate with nitrous oxide and carbon monoxide over heterogeneous catalysts containing both rhodium and iron phosphate

Qiang Yuan, Qinghong Zhang, Ye Wang *

*State Key Laboratory of Physical Chemistry of Solid Surfaces and Department of Chemistry, College of Chemistry and Chemical Engineering, Xiamen University, Xiamen 361005, China*

Received 2 February 2005; revised 19 April 2005; accepted 21 April 2005

Available online 31 May 2005

**Abstract**

The formation of methyl acetate during the conversion of $CH_4$ with $N_2O$ and CO over heterogeneous catalysts containing both rhodium and iron phosphate was studied. For two series of Rh-doped $FePO_4$ catalysts prepared by different methods, the optimum atomic ratios of Rh/Fe for methyl acetate formation are 1:600–1:400. The Rh–$FePO_4$ catalyst prepared from a mixed aqueous solution exhibits a higher rate and turnover frequency for methyl acetate formation than the Rh/$FePO_4$ prepared by the impregnation method. Characterizations with XRD, diffuse-reflectance UV–vis, TEM, and $H_2$-TPR suggest that $Rh^{3+}$ ions are mainly incorporated into the lattice of $FePO_4$ in the Rh–$FePO_4$ prepared from the mixed aqueous solution, whereas Rh(III) species probably exist on the surface of $FePO_4$ in the Rh/$FePO_4$ prepared by impregnation. The support of Rh(III) species and $FePO_4$ by MCM-41 by a co-impregnation method can drastically increase the rate and turnover frequency for methyl acetate formation, whereas a two-step impregnation method leads to catalysts without methyl acetate formation. The dual site containing Rh(III) species and $FePO_4$ in close proximity is proposed to account for methyl acetate formation. A possible reaction mechanism has been proposed on the basis of kinetic investigations.


*Keywords:* Methane; Oxidative carbonylation; Methyl acetate; Nitrous oxide; Rhodium; Iron phosphate; MCM-41

## 1. Introduction

Selective conversion of $CH_4$ to more valuable products that are particularly useful oxygenates is one of the biggest challenges for catalysis. The remarkably lower reactivity of $CH_4$ compared with that of the target product, such as $CH_3OH$ or HCHO, makes it highly difficult to develop a direct catalytic process with a satisfactory combination of high conversion and selectivity. Considerable effort has been devoted to the search for effective catalysts for the selective oxidation or oxidative functionalization of $CH_4$ to useful oxygenates [1–13], and some interesting homogeneous catalytic systems have been reported in recent years [4–7,11, 13–19].

Among the homogeneous catalytic transformations of $CH_4$, the oxidative carbonylation (or carboxylation) of $CH_4$ with CO in the presence of an oxidant (e.g., $K_2S_2O_8$) to form acetic acid in a single step,

$$CH_4 + CO + \text{oxidant} \rightarrow CH_3COOH + \text{reduced oxidant}, \quad (1)$$

has attracted much attention [20–29]. Acetic acid is an important chemical and is produced mainly by the carbonylation of methanol, as typically demonstrated in the Monsanto process in industry. If acetic acid or its derivatives such as methyl acetate can be produced directly from $CH_4$, the production costs for many chemical products based on acetic acid will be significantly reduced. Although several effective homogeneous catalysts have been reported for the direct

* Corresponding author. Fax: +86 592 2183047.
*E-mail address:* yewang@jingxian.xmu.edu.cn (Y. Wang).

0021-9517/$ – see front matter 
doi:10.1016/j.jcat.2005.04.025

oxidative carbonylation of $CH_4$ into acetic acid, none have met the requirements for commercialization as of this moment. High yields of acetic acid were reported with $K_2S_2O_8$ as the oxidant and $VO(acac)_2$ or $CaCl_2$ as the catalyst, but the turnover frequency (TOF) was low ($< 5\ h^{-1}$) [25,26]. Moreover, it was shown that the $CF_3COOH$, which was used as a solvent in these studies, might be involved in the formation of acetic acid by

$$CH_4 + CF_3COOH \rightarrow CH_3COOH + CF_3H, \quad (2)$$

and $CO_2$ was also produced in a large amount via radical reactions of $K_2S_2O_8$ with $CF_3COOH$ [27–29]. The consumption of both $K_2S_2O_8$ and $CF_3COOH$ would decrease the significance and the viability of these catalytic systems. For other systems using $O_2$ or $H_2O_2$ as the oxidant, the TOF for acetic acid formation was very low (e.g., ca. 0.4 $h^{-1}$ catalyzed by $RhCl_3$/KI [22] and ca. 1.3 $h^{-1}$ catalyzed by $NaVO_3$ [24]). The separation of expensive catalysts such as $RhCl_3$ from the products also presented a problem.

As compared with the complicated homogeneous systems, a simple heterogeneous catalytic system would be more desirable. Thus far, only scattered studies have contributed to the heterogeneous catalysis for the carbonylation of $CH_4$ or the conversion of $CH_4$ to acetic acid or its derivatives. The non-oxidative carbonylation of $CH_4$ to acetaldehyde or acetic acid with either CO or $CO_2$ is thermodynamically unfavorable. To overcome the thermodynamic limitations, two-step methods including (i) $CH_4$ decomposition on a metal catalyst to form carbonaceous species ($CH_x$) and (ii) reaction of CO or $CO_2$ with the adsorbed $CH_x$ to produce acetaldehyde or acetic acid were developed [30,31]. By using such a two-step method, Huang et al. [31] obtained a maximum rate of ca. 45 $\mu mol\ g^{-1}\ h^{-1}$ for acetic acid formation over a Cu–Co-based catalyst. Wilcox et al. [32] observed the adsorbed acetic acid species via diffuse-reflectance FTIR when a Pd/carbon or a $Pt/Al_2O_3$ was exposed to a mixture of $CH_4$ and $CO_2$, and the formation of gas-phase acetic acid with a yield of ca. $1.5 \times 10^{-6}$ during a temperature-programmed reaction of $CH_4$ and $CO_2$ over the $Pt/Al_2O_3$. Maeda et al. [33] found the formation of acetaldehyde during a temperature-programmed reaction of CO with the surface carbonaceous species (generated from $CH_4$ beforehand) in the presence of NO over a $Rh/SiO_2$. Li et al. [34] investigated the conversion of $CH_4$ in the presence of $CO_2$ with the use of plasma (dielectric-barrier discharge) and obtained mainly higher hydrocarbons and some oxygenates, including acetic acid with a maximum selectivity of 6%.

In a short communication [35], one of the present authors and his previous co-workers reported that $CH_4$ could be converted directly to methyl acetate in a single step via the reaction with $N_2O$ and CO over a Rh-doped $FePO_4$ catalyst

$$2CH_4 + N_2O + CO \rightarrow CH_3COOCH_3 + N_2 + H_2O. \quad (3)$$

Other transition-metal (e.g., Co, Ir, Ni, Pd, Ru, or Re)-doped $FePO_4$ samples and many Rh-doped metal oxides (e.g., $SiO_2$, $Al_2O_3$, $MoO_3$, and $V_2O_5$) or molecular sieves (e.g., HZSM-5) were also tested as catalysts for this reaction, but none exhibited significant activity for methyl acetate formation. Although the rate and TOF for methyl acetate formation are still low over the Rh-doped $FePO_4$ catalyst (ca. 30 $\mu mol\ g^{-1}\ h^{-1}$ and 2 $h^{-1}$ based on Rh, respectively) [35], the elucidation of catalyst requirements for methyl acetate formation is of significance from a fundamental chemical viewpoint. In the present paper, we report our recent studies on the clarification of the nature of the active sites for methyl acetate formation by comparing the performances of the Rh and $FePO_4$-based catalysts prepared by different methods. A possible reaction mechanism is also assessed by kinetic analysis.

## 2. Experimental

### 2.1. Catalyst preparation

Two series of Rh-doped $FePO_4$ samples were prepared by two different methods. The sample denoted as Rh-$FePO_4$ was prepared from a mixed aqueous solution containing $Rh(NO_3)_3$, $Fe(NO_3)_3$, and $NH_4H_2PO_4$ with a modified procedure for the preparation of $FePO_4$ [36]. The atomic ratio of Rh/Fe was varied from 1:800 to 1:60, and that of Fe/P was kept at 1:1. The mixed aqueous solution was heated at 343 K for ca. 6 h with continuous stirring. The reaction between $Rh(NO_3)_3$, $Fe(NO_3)_3$, and $NH_4H_2PO_4$ probably occurred during this process, and a gel was finally obtained. The gel was dried at 393 K and crushed to a fine powder. The powdery sample was finally calcined at 823 K in air for 6 h. On the other hand, the sample denoted as Rh/$FePO_4$ was prepared by the wet impregnation method. $FePO_4$ was first prepared with the procedure described above without the addition of $Rh(NO_3)_3$ [36]. Then the powdery $FePO_4$ was impregnated with an aqueous solution of $Rh(NO_3)_3$ at room temperature, followed by drying at 393 K and calcination at 823 K in air for 6 h.

MCM-41 was prepared by hydrothermal synthesis at 393 K for 96 h with sodium silicate and hexadecyltrimethylammonium bromide as the silica source and the template, respectively. The details of the procedure were described in our previous papers [37,38]. After hydrothermal synthesis, the resultant solid was thoroughly washed with deionized water, dried at 313 K in vacuum for 20 h, and finally calcined at 823 K in air for 6 h.

MCM-41-supported Rh-$FePO_4$ samples (denoted Rh-$FePO_4$/MCM-41) were prepared by a co-impregnation method. The procedure was similar to that for the preparation of $FePO_4$/MCM-41 [39]. Powdery MCM-41 was immersed in a mixed aqueous solution containing $Rh(NO_3)_3$, $Fe(NO_3)_3$, and $NH_4H_2PO_4$ and was allowed to stir for ca. 12 h at room temperature. The atomic ratio of Fe/P was kept at 1:1, and that of Rh/Fe was varied from 1:600 to 1:40. The slurry was then heated at 343 K with continu-

ous stirring. The resultant was further dried at 393 K for ca. 6 h and was finally calcined at 823 K in air for 6 h. In addition to the co-impregnation, a two-step impregnation method was also used for the preparation of the MCM-41-supported samples denoted as $Rh/FePO_4$/MCM-41. In the first step, we prepared $FePO_4$/MCM-41 by impregnating MCM-41 with a mixed aqueous solution of $Fe(NO_3)_3$ and $NH_4H_2PO_4$, followed by drying at 393 K and calcination at 823 K in air for 6 h. Subsequently, rhodium was introduced to the $FePO_4$/MCM-41 by a further impregnation with $Rh(NO_3)_3$ aqueous solution in the second step. The sample was finally calcined at 823 K in air for 6 h after drying at 393 K.

### 2.2. Catalyst characterization

Powder X-ray diffraction (XRD) patterns were measured with a Philips X'Pert Pro Super X-ray diffractometer equipped with X'Celerator and Xe detection systems. Cu-$K_\alpha$ radiation (40 kV and 40 mA) was used as the X-ray source.

$N_2$ physisorption at 77 K was carried out with a TriStar 3000 Surface Area and Porosimetry Analyzer (Micromeritics Instrument Co.) to examine the porosity and the surface area of each sample. All of the samples were pretreated at 573 K in vacuum for 3 h before $N_2$ adsorption. The pore diameter distribution was evaluated from the desorption branch of the adsorption/desorption isotherms by the BJH method.

Diffuse-reflectance UV–visible (UV–vis) spectra were recorded with a Varian-Cary 5000 spectrometer equipped with a diffuse-reflectance accessory. The spectra were collected at 200–800 nm with $BaSO_4$ as a reference.

Transmission electron microscopy (TEM) was done with a FEI Tecnai 30 electron microscope (Phillips Analytical) operated at an acceleration voltage of 300 kV. Samples for TEM measurements were suspended in ethanol and ultrasonically dispersed. Drops of the suspensions were applied on a copper grid coated with carbon.

X-ray photoelectron spectroscopy (XPS) was done with a Multilab 2000 system (Thermo Electron Co.) and Al-$K_\alpha$ radiation (1846.6 eV). Binding energies were corrected from charge effects by reference to the C1*s* peak of carbon contamination at 284.6 eV and measured with a precision of $\pm 0.2$ eV.

$H_2$-temperature-programmed reduction ($H_2$-TPR) was performed with an AutoChem 2920 II instrument (Micromeritics Instrument Co.). Typically, the sample (ca. 100 mg) loaded in a quartz reactor was first pretreated with a gas flow containing $O_2$ and He at 823 K for 1 h, followed by purging with pure He at the same temperature for 1 h. After the sample was cooled to 303 K, a $H_2$–Ar gas mixture (10% $H_2$) was introduced into the reactor, and the temperature was raised to 1273 K at a rate of 10 K $min^{-1}$. The consumption of $H_2$ was monitored with a thermal conductivity detector (TCD).

### 2.3. Catalytic reaction

The catalytic reactions were carried out in a fixed-bed flow reactor operated at atmospheric pressure. The catalyst was pretreated in the quartz reactor (inner diameter 8 mm) with a gas flow containing high-purity $N_2$ (99.999%, 50 $cm^3\,min^{-1}$) and $O_2$ (99.99%, 10 $cm^3\,min^{-1}$) at 823 K for 1 h, followed by purging with the high-purity $N_2$ (60 $cm^3\,min^{-1}$) at the same temperature for 1 h before reaction. We started the reaction by introducing a reactant gas flow containing $CH_4$ (99.995%), CO (> 99.99%), and $N_2O$ (> 99.99%) to the reactor after the temperature at the catalyst bed had decreased to the desired reaction temperature (648–773 K). The products were analyzed by three on-line gas chromatographs. All of the lines and valves between the exit of the reactor and the gas chromatographs were heated to 393 K to prevent condensation of the products. $CH_3OH$ and $CH_3COOCH_3$ in the products were separated with a Porapak T column and were detected with a FID detector. The separation and detection of other components such as $O_2$, $N_2$, $CH_4$, CO, and $CO_2$ were carried out with Porapak Q and Molecular Sieve 5 A columns and two TCD detectors. We confirmed no formation of acetic acid. The results after 1 h of reaction were typically shown and used for discussion, unless otherwise stated.

In addition to the reaction shown in Eq. (3), the following reactions may also take place over the catalysts investigated

$$CH_4 + N_2O \rightarrow CH_3OH\ (HCHO) + N_2, \tag{4}$$

$$CH_4 + 4N_2O \rightarrow CO_2\ (\text{or CO}) + 4N_2 + 2H_2O, \tag{5}$$

$$CO + N_2O \rightarrow CO_2 + N_2. \tag{6}$$

$N_2O$ conversion was evaluated from the amount of $N_2$ formed and of $N_2O$ remaining in the effluent. However, because $CO_2$ may be produced both from $CH_4$ and from CO, and CO may also be produced from $CH_4$, it is difficult to evaluate the conversions of $CH_4$ and CO, and the selectivities for $CH_3OH$, $CH_3COOCH_3$, and other products. Moreover, only a minor amount of HCHO was formed over most of the catalysts investigated in this study. Therefore, in this paper, we discuss our results with the formation rates of $CH_3OH$ and $CH_3COOCH_3$ and the TOF for $CH_3COOCH_3$ formation based on rhodium.

## 3. Results and discussion

### 3.1. Rh-doped $FePO_4$ catalysts

#### 3.1.1. Catalytic properties of the samples prepared by different methods

Table 1 compares the formation rates of $CH_3OH$ and $CH_3COOCH_3$ during the conversion of $CH_4$ with $N_2O$ and CO at 723 K over the two series of Rh-doped $FePO_4$ samples, that is, Rh–$FePO_4$ and $Rh/FePO_4$ with different

Table 1
Catalytic results of Rh-doped $FePO_4$ samples prepared by different methods for the conversion of $CH_4$ with $N_2O$ and CO[a]

| Catalyst[b] | Rh/Fe | Surface area ($m^2\,g^{-1}$) | $N_2O$ conversion (%) | Formation rate ($\mu mol\,g^{-1}\,h^{-1}$) | | TOF for $CH_3COOCH_3$ ($h^{-1}$) |
|---|---|---|---|---|---|---|
| | | | | $CH_3OH$ | $CH_3COOCH_3$ | |
| $FePO_4$ | – | 4.6 | 8.1 | 585 | 0 | 0 |
| 0.085% $Rh/FePO_4$ | 1/800 | 7.1 | 5.0 | 380 | 10.6 | 1.24 |
| 0.11% $Rh/FePO_4$ | 1/600 | 7.2 | 3.9 | 260 | 26.6 | 2.49 |
| 0.17% $Rh/FePO_4$ | 1/400 | 6.5 | 3.8 | 206 | 27.3 | 1.65 |
| 0.34% $Rh/FePO_4$ | 1/200 | 6.5 | 3.9 | 211 | 20.4 | 0.63 |
| 0.68% $Rh/FePO_4$ | 1/100 | 6.5 | 6.0 | 276 | 6.3 | 0.09 |
| 1.1% $Rh/FePO_4$ | 1/60 | 3.2 | ∼100 | 0 | 0 | 0 |
| 0.085% Rh–$FePO_4$ | 1/800 | 4.2 | 8.1 | 466 | 16.5 | 1.99 |
| 0.11% Rh–$FePO_4$ | 1/600 | 3.6 | 6.8 | 517 | 65.4 | 6.12 |
| 0.17% Rh–$FePO_4$ | 1/400 | 4.6 | 6.3 | 535 | 51.7 | 3.12 |
| 0.34% Rh–$FePO_4$ | 1/200 | 3.4 | 6.6 | 530 | 53.5 | 1.65 |
| 0.68% Rh–$FePO_4$ | 1/100 | 4.6 | 8.0 | 502 | 14.1 | 0.21 |
| 1.1% Rh–$FePO_4$ | 1/60 | 6.8 | 12 | 637 | 13.7 | 0.12 |

[a] Reaction conditions: catalyst, 0.2 g; temperature, 723 K; $P(CH_4) = 52.9$ kPa; $P(N_2O) = 16.5$ kPa; $P(CO) = 31.9$ kPa; total flow rate, 53.4 $cm^3\,min^{-1}$.
[b] The number before % denotes rhodium content in weight percentage.

rhodium content. $FePO_4$ without rhodium catalyzed the formation of $CH_3OH$, but no $CH_3COOCH_3$ was observed, suggesting that rhodium was indispensable for the formation of $CH_3COOCH_3$. The addition of rhodium to $FePO_4$ by the impregnation method ($Rh/FePO_4$ series) remarkably decreased the rate of $CH_3OH$ formation. $N_2O$ conversion was also decreased with the addition of rhodium up to 0.34 wt% (Rh/Fe = 1:200). The presence of rhodium, however, induced the formation of $CH_3COOCH_3$. With an increase in rhodium content from 0 to 0.17 wt% (Rh/Fe = 1:400), the rate of $CH_3COOCH_3$ formation increased and reached a maximum of 27.3 $\mu mol\,g^{-1}\,h^{-1}$ at a rhodium content of 0.17 wt%. The maximum TOF (2.49 $h^{-1}$) for $CH_3COOCH_3$ formation was observed at a rhodium content of 0.11 wt% (Rh/Fe = 1:600). A further increase in rhodium content from 0.17 to 0.68 wt% decreased both the rate and the TOF for $CH_3COOCH_3$ formation, although the formation of $CH_3OH$ could be kept or enhanced slightly. Neither $CH_3COOCH_3$ nor $CH_3OH$ was obtained as the rhodium content was increased to 1.1 wt%. A big increase in $N_2O$ conversion to nearly 100% was observed simultaneously, indicating the predominant occurrence of the reaction (6), that is, the reduction of $N_2O$ by CO.

On the other hand, for the Rh–$FePO_4$ series of samples prepared from the mixed aqueous solution, the presence of rhodium with a content of 0.085–0.68 wt% decreased the rate of $CH_3OH$ formation and $N_2O$ conversion only slightly. Such decreases were apparently smaller as compared with those for the $Rh/FePO_4$ series of samples. The presence of rhodium also induced the formation of $CH_3COOCH_3$. At a rhodium content of 0.11 wt% (Rh/Fe = 1:600), the rate and TOF for $CH_3COOCH_3$ formation arrived at maximum values of 65.4 $\mu mol\,g^{-1}\,h^{-1}$ and 6.12 $h^{-1}$, respectively. These maximum values were both significantly higher than those observed for the $Rh/FePO_4$ series of catalysts. Similar to the tendency observed for the $Rh/FePO_4$ series of catalysts, a further increase in rhodium content above 0.11 wt% was detrimental to the formation of $CH_3COOCH_3$. As compared with the 0.11 wt% $Rh/FePO_4$, the BET surface area of the 0.11 wt% Rh–$FePO_4$ catalyst was rather lower, suggesting that the catalytic performances had no relations with the surface area.

To make a further comparison between the two series of catalysts, temperature dependences of catalytic performances over both the Rh–$FePO_4$ and the $Rh/FePO_4$ samples with a Rh content of 0.11 wt% were investigated. As shown in Fig. 1, the increase in reaction temperature in the range of 648–763 K raised the rates of $CH_3OH$ formation monotonically over both catalysts. However, the rate of $CH_3COOCH_3$ formation increased to a maximum with a rise in reaction temperature and then decreased with a further increase in temperature over each catalyst (Fig. 1A). The same tendency was observed for the change in the TOF for $CH_3COOCH_3$ formation with reaction temperature (Fig. 1B). The rate and TOF for $CH_3COOCH_3$ formation were higher over the Rh–$FePO_4$ catalyst in the whole temperature range investigated. Moreover, the ratio of $CH_3COOCH_3/CH_3OH$ at temperatures of 648–723 K was also higher over the Rh–$FePO_4$ catalyst.

### *3.1.2. Characterizations of the samples prepared by different methods*

Fig. 2 shows the XRD patterns for several typical Rh-doped $FePO_4$ samples prepared by different methods, as well as for $FePO_4$. $FePO_4$ without rhodium showed a quartz-like crystalline structure (curve a). For all of the Rh-doped $FePO_4$ samples investigated, no crystalline phase related to rhodium or rhodium oxide could be detected, because the maximum rhodium content was only 1.1 wt%. The two series of samples, however, exhibited different XRD patterns. The $Rh/FePO_4$ samples prepared by the impregnation method showed the same XRD pattern as $FePO_4$. However, as compared with $FePO_4$ or the $Rh/FePO_4$ samples, the Rh–$FePO_4$ samples prepared from the mixed aqueous solution

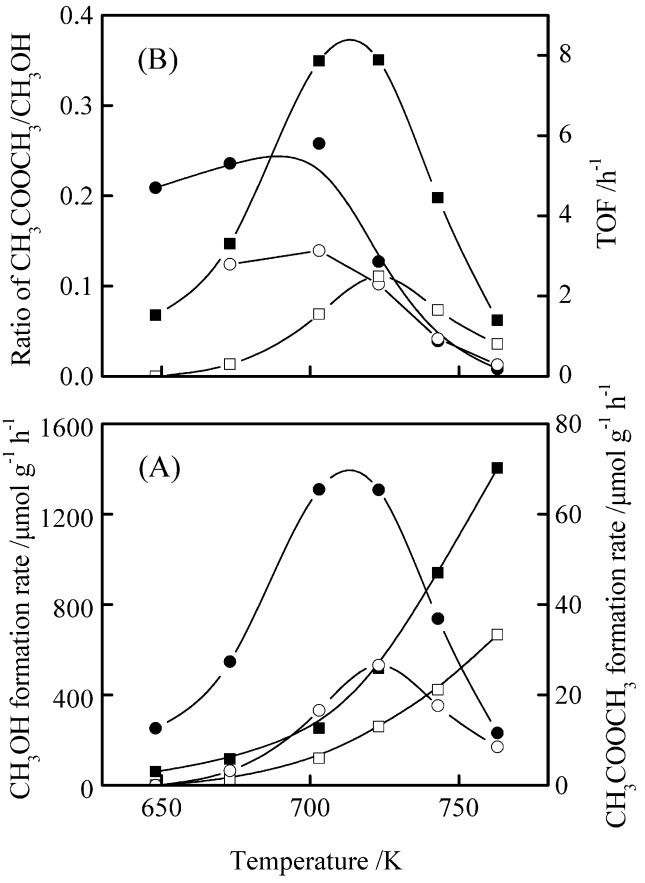


Fig. 1. Comparisons of catalytic performances of the Rh–$FePO_4$ and Rh/$FePO_4$ samples with rhodium content of 0.11 wt%. Solid and empty marks are for the Rh–$FePO_4$ and the Rh/$FePO_4$, respectively. (A) (■ and □), methanol formation rate; (● and ○), $CH_3COOCH_3$ formation rate. (B) (● and ○), ratio of $CH_3COOCH_3$ to $CH_3OH$; (■ and □), TOF. Reaction conditions: catalyst, 0.2 g; $P(CH_4) = 52.9$ kPa; $P(N_2O) = 16.5$ kPa; $P(CO) = 31.9$ kPa; total flow rate, 53.4 $cm^3$ $min^{-1}$.

exhibited remarkably lower intensity for the strongest peak of the quartz-like phase ($2\theta = 25.8°$). Moreover, new diffraction peaks appeared at 21.1°, 22.8°, and 27.0° for this series of samples, and these peaks became obvious as the rhodium content was increased to 1.1 wt% (curve e). These peaks, along with that at 20.2°, could be assigned to the tridymite-like phase of $FePO_4$ [39,40]. It was reported that the tridymite-like phase of $FePO_4$ was formed at a lower temperature (ca. 423 K) by calcination of a $FePO_4 \cdot 2H_2O$ precursor and was transformed to the quartz-like phase at 773–873 K during temperature-programmed heating at a rate of 5 K $min^{-1}$ [40]. The calcination of $FePO_4$ or the Rh/$FePO_4$ samples at 823 K for 6 h in our case caused the complete formation of the quartz-like phase of $FePO_4$. Thus, the lower intensity of the strongest peak of the quartz-like phase and the remainder of the tridymite-like phase in the case of Rh–$FePO_4$ series of samples suggest that rhodium in this series of samples probably exerts a larger influence on the crystalline structure of $FePO_4$.

Diffuse-reflectance UV–vis spectra of the two series of samples along with $FePO_4$ are shown in Fig. 3. Two bands at

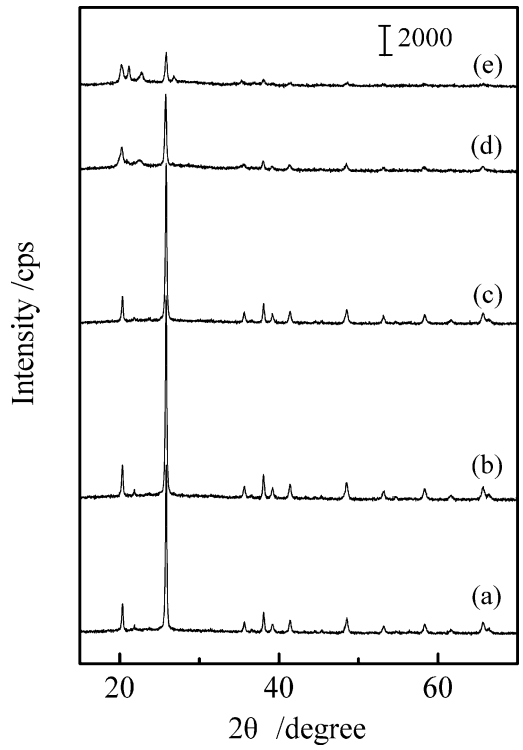


Fig. 2. XRD patterns of the Rh–$FePO_4$ and Rh/$FePO_4$ samples along with $FePO_4$. (a) $FePO_4$, (b) Rh/$FePO_4$ (Rh, 0.11 wt%), (c) Rh/$FePO_4$ (Rh, 1.1 wt%), (d) Rh–$FePO_4$ (Rh, 0.11 wt%), (e) Rh–$FePO_4$ (Rh, 1.1 wt%).

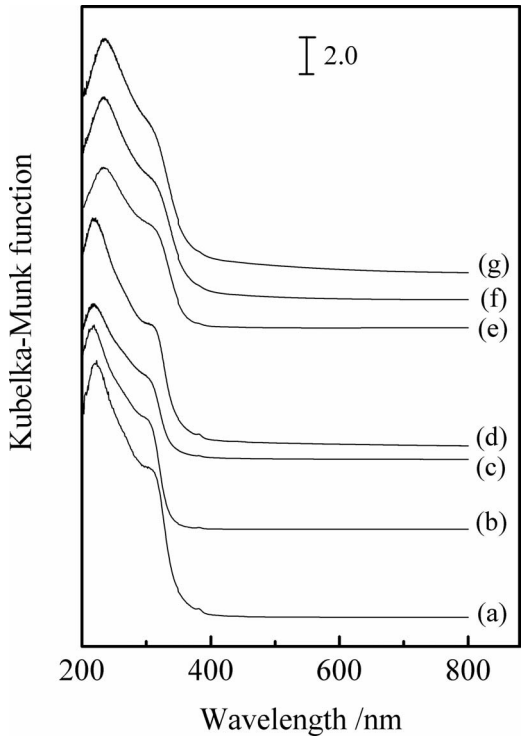


Fig. 3. Diffuse reflectance UV–vis spectra of the Rh–$FePO_4$ and Rh/$FePO_4$ samples along with $FePO_4$. (a) $FePO_4$, (b) Rh/$FePO_4$ (Rh, 0.11 wt%), (c) Rh/$FePO_4$ (Rh, 0.34 wt%), (d) Rh/$FePO_4$ (Rh, 1.1 wt%), (e) Rh–$FePO_4$ (Rh, 0.11 wt%), (f) Rh–$FePO_4$ (Rh, 0.34 wt%), (g) Rh–$FePO_4$ (Rh, 1.1 wt%).

Table 2
Bandgap energies for the allowed transitions of $FePO_4$ and Rh-doped $FePO_4$

| Sample[a] | $E_g$ (eV) | |
|---|---|---|
| | P–O | Fe–O |
| $FePO_4$ | 3.64 | 4.25 |
| 0.11% Rh/$FePO_4$ | 3.67 | 4.25 |
| 0.34% Rh/$FePO_4$ | 3.62 | 4.22 |
| 1.1% Rh/$FePO_4$ | 3.66 | 4.28 |
| 0.11% Rh–$FePO_4$ | 3.59 | 4.18 |
| 0.34% Rh–$FePO_4$ | 3.58 | 4.11 |
| 1.1% Rh–$FePO_4$ | 3.55 | 4.00 |

[a] The number before % denotes rhodium content in weight percentage.

225 and 310 nm were observed for $FePO_4$ without rhodium (curve a). Since $P_2O_5$ and $NH_4H_2PO_4$ possessed an absorption band at ca. 230 nm, the two bands observed for $FePO_4$ were assigned to the charge transfer transitions of P–O and Fe–O, respectively. The introduction of rhodium into $FePO_4$ by the impregnation method (Rh/$FePO_4$ series) did not significantly change the positions of these two bands (curves b–d). However, for the Rh–$FePO_4$ series of samples prepared from the mixed aqueous solution, the two bands both shifted to longer wavelength positions because of the presence of rhodium, and the peaks were observed at 235–240 and 315–320 nm, respectively (curves e–g).

It is known that the energy of the absorption edge reflects the bandgap energy ($E_g$) of an insulator or semiconductor [41]. We have calculated the bandgap energy values for both P–O and Fe–O bands from Fig. 3, using the method proposed by Weber [41], that is, by finding the energy intercepts of two straight lines in the plot of $[F(R_\infty) \times h\nu]^2$ against $h\nu$, where $F(R_\infty)$ is the Kubelka–Munk function and $h\nu$ is the incident photon energy. The results shown in Table 2 reveal that the bandgap energies for both absorption bands are decreased by the presence of rhodium for the Rh–$FePO_4$ series of samples, whereas they are almost not affected for the Rh/$FePO_4$ series of samples. Thus, it is clear that rhodium in the Rh–$FePO_4$ samples exerts a bigger influence on the electronic structure of $FePO_4$.

XPS results revealed that there were no significant differences in the binding energies of Fe2$p_{3/2}$, P2$p$, O1$s$, and Rh3$d_{5/2}$ between the two series of samples, indicating that the oxidation states of these elements in the two series of samples are the same. The binding energies of Fe2$p_{3/2}$, P2$p$, and O1$s$ were observed at 711.4–711.8, 133.1–133.3, and 530.9–531.1 eV, respectively. These values were almost the same as those for $FePO_4$ without rhodium. Fig. 4 shows Rh3$d$ spectra for some typical samples. The binding energies of Rh3$d_{5/2}$ for these samples were observed at 309.5–309.9 eV, which could be ascribed to rhodium in an oxidation state of +III [42]. Thus it is likely that rhodium species in these samples are in the state of $Rh^{3+}$ cations or $Rh_2O_3$ clusters.

TEM observations showed differences between the two series of samples. For the Rh–$FePO_4$ series of samples

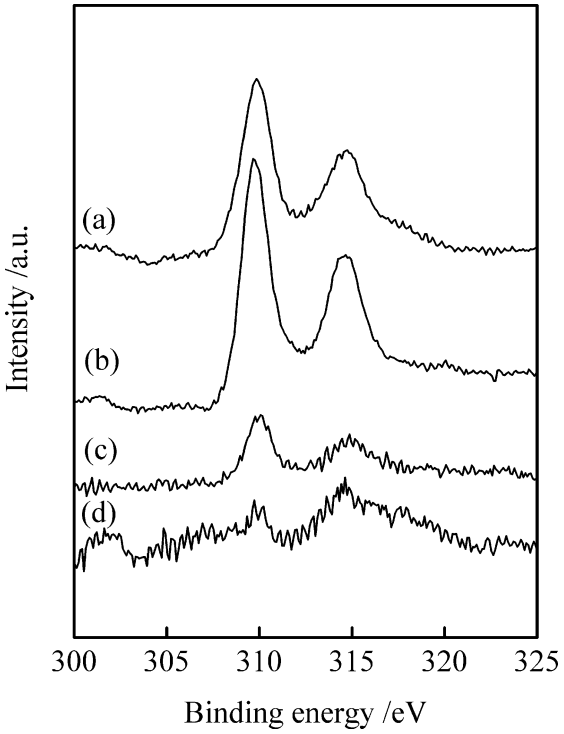


Fig. 4. Rh3$d$ XPS spectra of the Rh–$FePO_4$ and Rh/$FePO_4$ samples. (a) Rh–$FePO_4$ (Rh, 0.68 wt%), (b) Rh/$FePO_4$ (Rh, 0.68 wt%), (c) Rh–$FePO_4$ (Rh, 0.34 wt%), (d) Rh–$FePO_4$ (Rh, 0.34 wt%) after the reaction for 1 h under the conditions in Table 1.

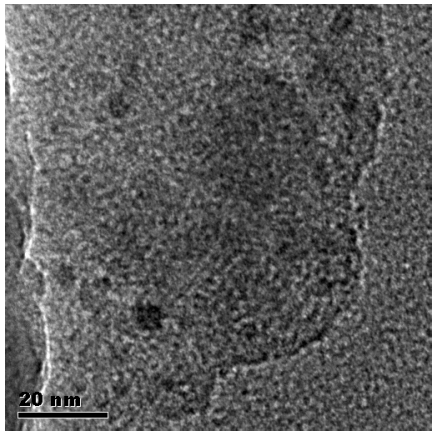


Fig. 5. TEM micrograph of the Rh/$FePO_4$ (Rh, 1.1 wt%) sample.

with a rhodium content in the range of 0.085–1.1 wt%, no rhodium oxide particles could be discerned in TEM images, indicating high dispersions of rhodium in this series of samples. On the other hand, as shown in Fig. 5, rhodium oxide particles with sizes of 2–6 nm were observable for the Rh/$FePO_4$ sample with a rhodium content of 1.1 wt%. Thus the aggregation of Rh(III) species or small $RhO_x$ clusters into $Rh_2O_3$ on the surface of $FePO_4$ particles probably occurred over this sample.

From the results obtained above, we speculate that $Rh^{3+}$ cations may be incorporated into the lattice of $FePO_4$ to substitute $Fe^{3+}$ cations in the Rh–$FePO_4$ series of samples,

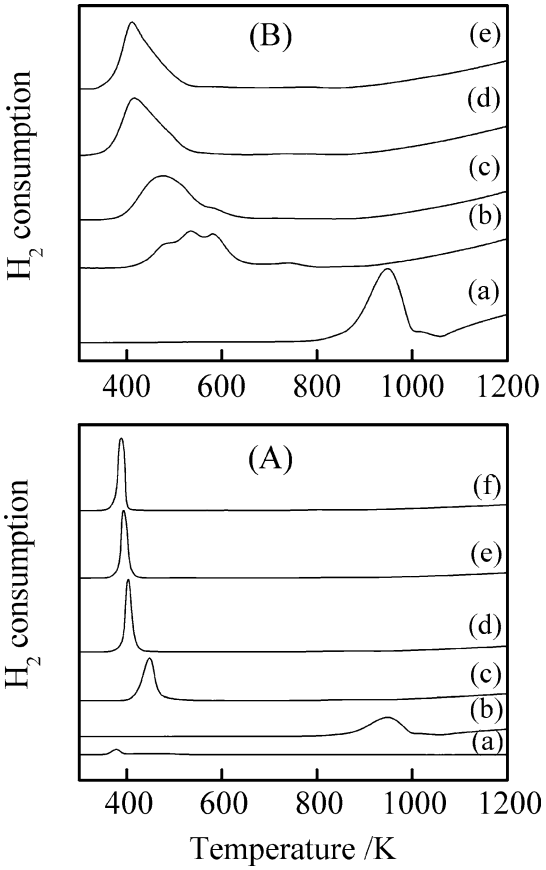


Fig. 6. $H_2$-TPR profiles of the Rh–$FePO_4$ and Rh/$FePO_4$ samples along with $Rh_2O_3$ and $FePO_4$. (A) (a) $Rh_2O_3$, (b) $FePO_4$, (c) Rh/$FePO_4$ (Rh, 0.11 wt%), (d) Rh/$FePO_4$ (Rh, 0.34 wt%), (e) Rh/$FePO_4$ (Rh, 0.68 wt%), (f) Rh/$FePO_4$ (Rh, 1.1 wt%). (B) (a) $FePO_4$, (b) Rh–$FePO_4$ (Rh, 0.11 wt%), (c) Rh–$FePO_4$ (Rh, 0.34 wt%), (d) Rh–$FePO_4$ (Rh, 0.68 wt%), (e) Rh–$FePO_4$ (Rh, 1.1 wt%).

whereas rhodium in the Rh/$FePO_4$ samples may be present mainly on the surface of $FePO_4$. The presence of $Rh^{3+}$ in the lattice of $FePO_4$ would bring about changes in both the lattice and the electronic structures, as reflected in Figs. 2 and 3. The surface Rh(III) species or small $RhO_x$ clusters in the Rh/$FePO_4$ samples may easily aggregate into $Rh_2O_3$ particles at a higher rhodium content (1.1 wt%), as shown by TEM observations (Fig. 5).

Such speculations have been further supported by $H_2$-TPR studies. $H_2$-TPR profiles for the two series of Rh-doped $FePO_4$ samples along with $FePO_4$ and $Rh_2O_3$ are shown in Fig. 6. The reduction of $Rh_2O_3$ to $Rh^0$ occurred at low temperatures with a peak at 378 K, and the reduction peak for $FePO_4$ was observed at 951 K, and it was confirmed that this peak corresponded to the reduction of $FePO_4$ to $Fe_2P_2O_7$ [39]. For each Rh/$FePO_4$ sample (Fig. 6A, curves c–f), a relatively sharp reduction peak was observed at 389–448 K. The reduction peak shifted to a lower temperature at a higher rhodium content. The quantitative calculation has clarified that the reduction peak observed for each Rh/$FePO_4$ sample includes both the reduction of $Rh^{3+}$ to $Rh^0$ and that of $FePO_4$ to $Fe_2P_2O_7$. Thus the peak temperature for the reduction of $FePO_4$ to $Fe_2P_2O_7$ was decreased by more than 500 K because of the presence of rhodium. The acceleration of the reduction of an oxide by a noble metal deposited on it is a well-known phenomenon for many systems such as Pt/$Fe_2O_3$ [43], and it is generally accepted that $H_2$ is dissociatively chemisorbed on the noble metal and the H atoms subsequently spill over to the metal oxide to enhance its reduction [44]. In our case, Rh(III) species or $RhO_x$ clusters on the surface of $FePO_4$ should first be reduced by $H_2$, and then the $Rh^0$ would activate $H_2$ molecules to H atoms. Since only one sharp reduction peak has been observed for each Rh/$FePO_4$ sample, it is reasonable to speculate that the H atoms are rapidly used in the reduction of $FePO_4$, probably through an efficient spillover process.

Although the presence of rhodium also greatly lowered the temperature for $FePO_4$ reduction for the Rh–$FePO_4$ samples (Fig. 6B, curves b–e), the reduction peaks of these samples were much broader. For the sample with a low rhodium content (0.11 wt%), even three reduction peaks could be observed. Moreover, the peak temperature for the Rh–$FePO_4$ was higher than that for the Rh/$FePO_4$ with the same rhodium content. We think that the broadening and the high-temperature shift of the reduction peak for the Rh–$FePO_4$ samples are supportive of the conclusion that $Rh^{3+}$ cations are mainly incorporated into the lattice of $FePO_4$ in these samples. The reduction of the isolated $Rh^{3+}$ dispersed in the lattice of $FePO_4$ by $H_2$ would become difficult compared with the Rh(III) species or $RhO_x$ clusters on the surface, leading to the high-temperature shift and the broadening of the reduction peak. The diffusion of $H_2$ molecules but not the spillover of H atoms to the lattice in the case of Rh–$FePO_4$ might also cause broadening of the reduction peak.

### 3.1.3. *Kinetic behavior of the Rh–$FePO_4$ catalyst*

To gain insight into the whole image of reactions, we carried out kinetic investigations over the Rh–$FePO_4$ catalyst with a Rh/Fe ratio of 1:600, which could give the best performance for methyl acetate formation. Fig. 7 shows the effect of the pseudo-contact time, expressed as $W/F$, on the amounts of $CH_3OH$ and $CH_3COOCH_3$ formed per hour at 723 K, where $W$ and $F$ denote the catalyst weight and the total flow rate, respectively. In this series of experiments, we varied the value of $W/F$ by changing the catalyst weight while keeping the flow rate at 100 $cm^3\,min^{-1}$. The amounts of $CH_3OH$ and $CH_3COOCH_3$ formed were both proportional to $W/F$ in the range investigated. The observations that the formation of $CH_3COOCH_3$ has not been accelerated and that of $CH_3OH$ has not been decelerated with contact time suggest that $CH_3COOCH_3$ may be formed not via the consecutive reaction of $CH_3OH$ but directly from $CH_4$ in parallel with $CH_3OH$.

Fig. 8 shows the effect of $CH_4$ partial pressure, expressed as $P(CH_4)$, on the formation rates of $CH_3OH$ and $CH_3COOCH_3$ at constant partial pressures of $N_2O$ and CO. At $P(CH_4) < 30$ kPa, the rate of $CH_3OH$ formation in-

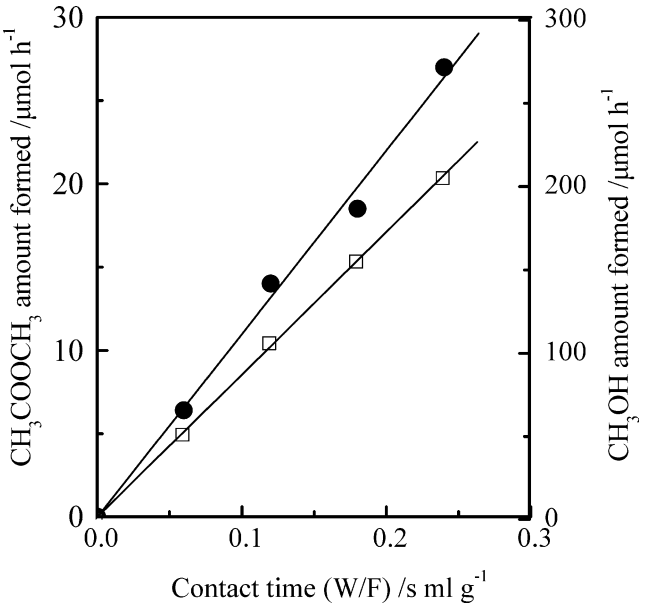


Fig. 7. Effect of the pseudo-contact time ($W/F$) on the amounts of $CH_3OH$ and $CH_3COOCH_3$ formed per hour over the Rh–$FePO_4$ (Rh, 0.11 wt%). (●) $CH_3COOCH_3$, (□) $CH_3OH$. Reaction conditions: temperature, 723 K; $P(CH_4) = 30.3$ kPa; $P(N_2O) = 20.2$ kPa; $P(CO) = 20.2$ kPa; total flow rate, 100 $cm^3\,min^{-1}$.

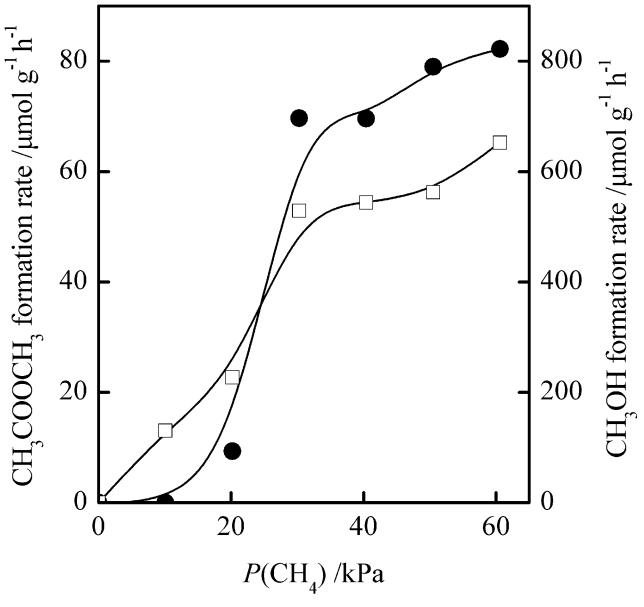


Fig. 8. Catalytic performances as a function of $CH_4$ partial pressure over the Rh–$FePO_4$ (Rh, 0.11 wt%). (●) Rate of $CH_3COOCH_3$ formation, (□) rate of $CH_3OH$ formation. Reaction conditions: catalyst, 0.2 g; temperature, 723 K; $P(N_2O) = 20.2$ kPa; $P(CO) = 20.2$ kPa; total flow rate, 100 $cm^3\,min^{-1}$.

creased almost linearly with $P(CH_4)$, suggesting a first-order dependence of $CH_3OH$ formation with respect to $CH_4$ in this region. In the same range of $P(CH_4)$, however, the rate of $CH_3COOCH_3$ formation depended on $P(CH_4)$ in a different manner. The curve for the rate of $CH_3COOCH_3$ formation at $P(CH_4) < 30$ kPa could be fitted with the assumption of a second-order dependence of $CH_3COOCH_3$

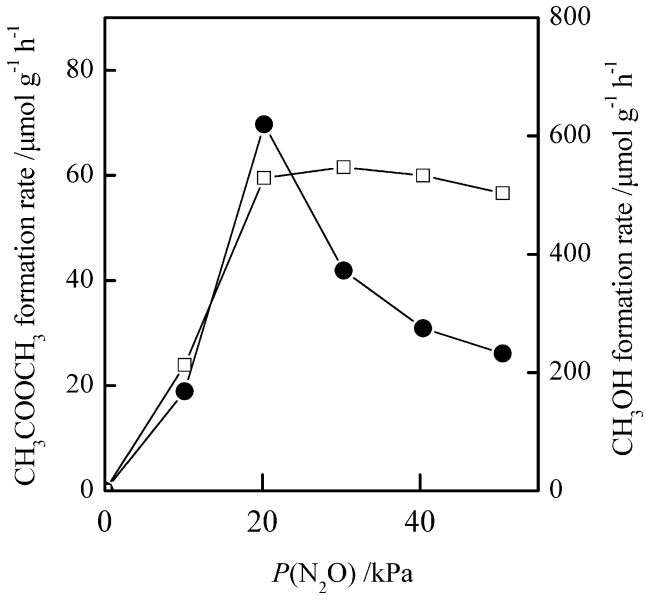


Fig. 9. Catalytic performances as a function of $N_2O$ partial pressure over the Rh–$FePO_4$ (Rh, 0.11 wt%). (●) Rate of $CH_3COOCH_3$ formation, (□) rate of $CH_3OH$ formation. Reaction conditions: catalyst, 0.2 g; temperature, 723 K; $P(CH_4) = 30.3$ kPa; $P(CO) = 20.2$ kPa; total flow rate, 100 $cm^3\,min^{-1}$.

formation with respect to $P(CH_4)$. This result supports the assumption that one $CH_3COOCH_3$ molecule is produced from two $CH_4$ molecules (Eq. (3)). The increase in $P(CH_4)$ above 30 kPa saturated the formation rates of both $CH_3OH$ and $CH_3COOCH_3$.

The formation rates of $CH_3OH$ and $CH_3COOCH_3$ as a function of $N_2O$ partial pressure, $P(N_2O)$, are shown in Fig. 9. The rate of $CH_3OH$ formation increased with an increase in $P(N_2O)$ from 0 to 20 kPa and was saturated with a further increase in $P(N_2O)$. On the other hand, there was a maximum for the rate of $CH_3COOCH_3$ formation at $P(N_2O)$ of 20 kPa. There are two possibilities for the decrease in the rate of $CH_3COOCH_3$ formation at higher $P(N_2O)$. One possibility is the rapid consecutive oxidation of the formed $CH_3COOCH_3$ to CO and $CO_2$ at higher $P(N_2O)$. The other possibility is the competition between the carbonylation of the $CH_3$ intermediate with CO to form an acetyl ($CH_3CO$) species, the precursor for $CH_3COOCH_3$ formation, and the oxidation of the $CH_3$ intermediate to the $CH_3O$ species and further to CO and $CO_2$. A higher $P(N_2O)$ would result in a higher concentration of oxygen species on the surface and would increase the probability of further oxidation of the $CH_3$ intermediate and decrease that of carbonylation.

Fig. 10 shows the effect of CO partial pressure, $P(CO)$, on catalytic results. No $CH_3COOCH_3$ was formed in the absence of CO, and thus CO played a key role in the formation of $CH_3COOCH_3$. It is of interest to note that $CH_3OH$ is also not formed over the Rh–$FePO_4$ catalyst under current conditions in the absence of CO. Only CO, $CO_2$, and a trace amount of HCHO were detectable over the current catalyst in the absence of CO, and $CH_3OH$, $CH_3OCH_3$, and HCHO

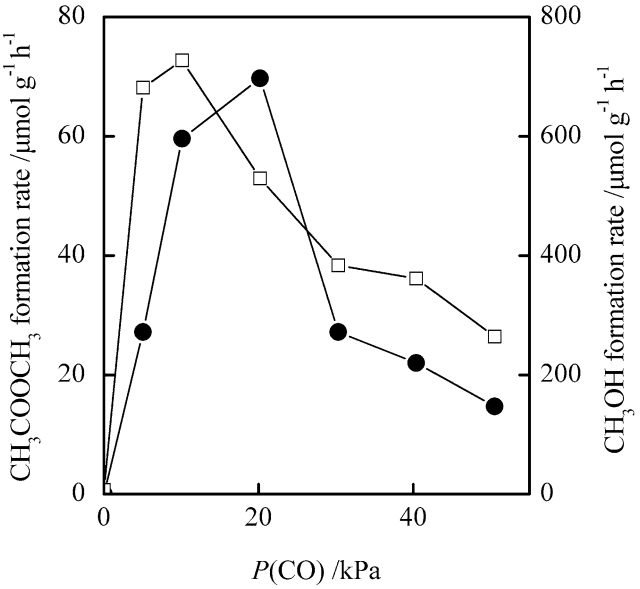


Fig. 10. Catalytic performances as a function of CO partial pressure over the Rh–$FePO_4$ (Rh, 0.11 wt%). (●) Rate of $CH_3COOCH_3$ formation, (□) rate of $CH_3OH$ formation. Reaction conditions: catalyst, 0.2 g; temperature, 723 K; $P(CH_4) = 30.3$ kPa; $P(N_2O) = 20.2$ kPa; total flow rate, 100 $cm^3$ $min^{-1}$.

were formed during the oxidation of $CH_4$ with $N_2O$ over $FePO_4$ [39]. The incorporation of rhodium into $FePO_4$ may accelerate the overoxidation of these oxygenates in the absence of CO. In the previous communication [35], where a different Rh-doped $FePO_4$ catalyst and different reaction conditions were used, the enhancement of $CH_3OH$ formation was also indicated by the presence of CO, although a small amount of $CH_3OH$ was formed in the absence of CO. The presence of CO increased the rate of $CH_3OH$ formation, possibly by enhancing the activation of $N_2O$ to active oxygen species for $CH_4$ conversion via a partial reduction of $Fe^{3+}$ to $Fe^{2+}$ on the surface and/or by lowering the overoxidation capacity of rhodium species through interactions with CO. In other words, the state of rhodium in the Rh–$FePO_4$ catalyst might be modified via interactions with CO. The increase in $P$(CO) above 10 kPa decreased the rate of $CH_3OH$ formation but still increased that of $CH_3COOCH_3$ formation, which showed a maximum at $P$(CO) of 20 kPa and then decreased sharply.

### 3.2. Catalytic and structural properties of MCM-41-supported Rh–$FePO_4$

In a previous paper we clarified that the small $FePO_4$ clusters encapsulated inside the mesoporous channels in MCM-41-supported $FePO_4$ samples exhibit higher catalytic performance for the selective oxidation of $CH_4$ by $N_2O$ to oxygenates than the crystalline $FePO_4$ [39]. Here the supporting effect of MCM-41 on the catalytic properties of the Rh–$FePO_4$ for the conversion of $CH_4$ to $CH_3COOCH_3$ with $N_2O$ and CO is investigated.

The catalytic results obtained for some MCM-41-supported samples are shown in Table 3. The content of $FePO_4$ in these samples was fixed at 9.1 wt%. The rate of $CH_3OH$ formation became remarkably higher (ca. 1.6 times) over the 9.1 wt% $FePO_4$/MCM-41 than that over the unsupported $FePO_4$. With the introduction of rhodium by the co-impregnation method to a certain content (0.017 wt%, Rh/Fe = 1:400), $CH_3COOCH_3$ began to appear. The rate of $CH_3COOCH_3$ formation increased rapidly with rhodium content and reached a maximum of 696 μmol $g^{-1}$ $h^{-1}$ at a rhodium content of 0.11 wt% (Rh/Fe = 1:60). The TOF for $CH_3COOCH_3$ formation reached 65.2 $h^{-1}$ simultaneously. Further optimizations of the rate and TOF for $CH_3COOCH_3$ formation produced by a change in the content of $FePO_4$ from 5 to 40 wt% and the atomic ratio of Rh/Fe from 1:600 to 1:40 have revealed that the 0.11 wt% Rh–9.1 wt% $FePO_4$/MCM-41 catalyst possesses the highest activity for $CH_3COOCH_3$ formation. As compared with the best unsupported Rh–$FePO_4$ catalyst (Rh, 0.11 wt%), the rate and TOF for $CH_3COOCH_3$ formation have increased ca. 10 and 8 times, respectively. To the best of our knowledge, these values are both the highest for the oxidative carbonylation of $CH_4$ over all of the catalytic systems (including homogeneous systems) reported so far. It is also of significance that the ratio of $CH_3COOCH_3$ to $CH_3OH$ observed here has increased considerably as compared with the unsupported catalysts. This probably suggests that the carbonylation can proceed with a remarkably higher probability over

Table 3
Catalytic results of MCM-41-supported Rh and $FePO_4$ samples for the conversion of $CH_4$ with $N_2O$ and CO[a]

| Catalyst[b] | Rh/Fe | Surface area ($m^2$ $g^{-1}$) | Pore diameter (nm) | $N_2O$ conversion (%) | Formation rate (μmol $g^{-1}$ $h^{-1}$) | | TOF for $CH_3COOCH_3$ ($h^{-1}$) |
|---|---|---|---|---|---|---|---|
| | | | | | $CH_3OH$ | $CH_3COOCH_3$ | |
| 9.1% $FePO_4$/MCM-41 | – | 830 | 3.2 | 13 | 945 | 0 | 0 |
| 0.011% Rh–9.1% $FePO_4$/MCM-41 | 1/600 | 836 | 3.1 | 13 | 926 | Trace | Trace |
| 0.017% Rh–9.1% $FePO_4$/MCM-41 | 1/400 | 803 | 3.1 | 14 | 909 | 4.4 | 2.65 |
| 0.068% Rh–9.1% $FePO_4$/MCM-41 | 1/100 | 801 | 3.0 | 82 | 1202 | 380 | 57.5 |
| 0.11% Rh–9.1% $FePO_4$/MCM-41 | 1/60 | 802 | 2.9 | 99 | 587 | 696 | 65.2 |
| 0.17% Rh–9.1% $FePO_4$/MCM-41 | 1/40 | 803 | 2.9 | 99 | 673 | 349 | 21.1 |
| 0.11% Rh/9.1% $FePO_4$/MCM-41[c] | 1/60 | 800 | 2.9 | ∼100 | 0 | 0 | 0 |

[a] Reaction conditions: catalyst, 0.2 g; temperature, 723 K; $P(CH_4) = 52.9$ kPa; $P(N_2O) = 16.5$ kPa; $P$(CO) = 31.9 kPa; total flow rate, 53.4 $cm^3$ $min^{-1}$.
[b] The numbers before % Rh and % $FePO_4$ denote rhodium and $FePO_4$ contents in weight percentage in each sample.
[c] The sample was prepared by the two-step impregnation method.

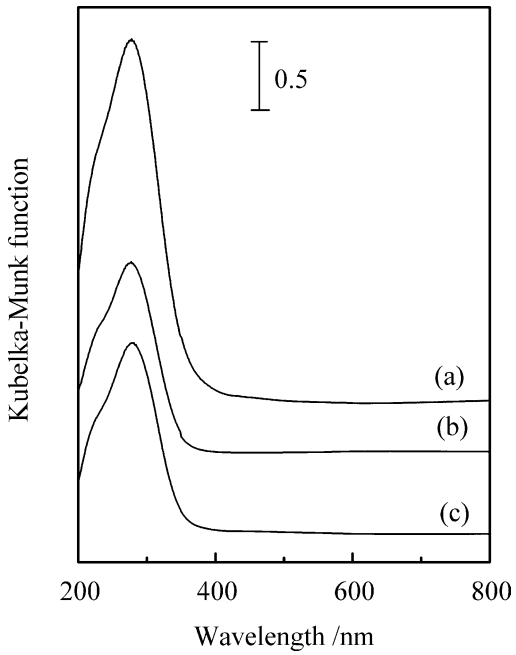


Fig. 11. Diffuse reflectance UV–vis spectra of MCM-41-supported samples. (a) 9.1 wt% $FePO_4$/MCM-41, (b) 0.11 wt% Rh/9.1 wt% $FePO_4$/MCM-41 (two step impregnation), (c) 0.11 wt% Rh–9.1 wt% $FePO_4$/MCM-41 (co-impregnation).

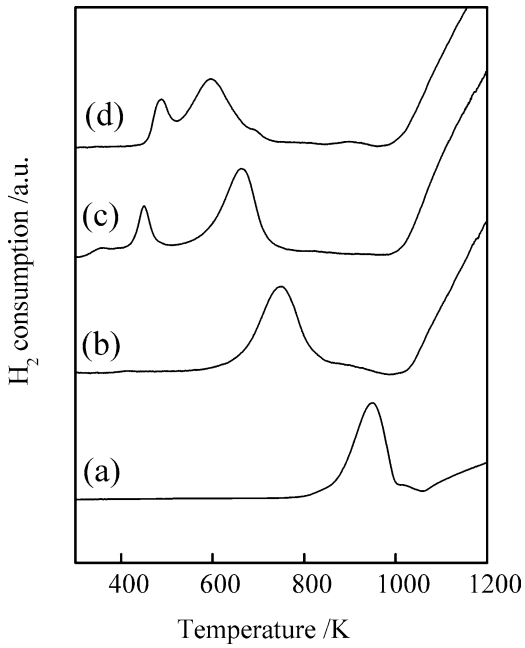


Fig. 12. $H_2$-TPR profiles of MCM-41-supported samples along with $FePO_4$. (a) $FePO_4$, (b) 9.1 wt% $FePO_4$/MCM-41, (c) 0.11 wt% Rh/9.1 wt% $FePO_4$/MCM-41 (two step impregnation), (d) 0.11 wt% Rh–9.1 wt% $FePO_4$/MCM-41 (co-impregnation).

the MCM-41-supported catalyst with an appropriate Rh/Fe ratio.

On the other hand, the 0.11 wt% Rh/9.1 wt% $FePO_4$/MCM-41 sample prepared by the two-step impregnation did not catalyze the formation of $CH_3COOCH_3$. Even $CH_3OH$ was not produced over this catalyst. $N_2O$, however, was completely consumed, and a large amount of $CO_2$ was formed. Thus, this sample predominantly catalyzed the reduction of $N_2O$ with CO (reaction (6)) under the reaction conditions used.

We have carried out characterizations to uncover the structural differences between the Rh–$FePO_4$/MCM-41 and the Rh/$FePO_4$/MCM-41 prepared by the co-impregnation and the two-step impregnation, respectively. XRD measurements showed that, for both samples, only a broad diffraction peak at ca. 23° due to the amorphous feature of the framework of MCM-41 appeared, and no peak of the crystalline $FePO_4$ could be observed. Fig. 11 shows diffuse-reflectance UV–vis spectra of the MCM-41-supported samples. The support of $FePO_4$ by MCM-41 changed the diffuse-reflectance UV–vis pattern. Instead of the bands observed at 225 and 310 nm for $FePO_4$ (Fig. 3), a main band was observed at 276 nm along with a shoulder at 218 nm for the 9.1 wt% $FePO_4$/MCM-41. We tentatively speculate that such a change is related to the encapsulation of $FePO_4$ inside the mesoporous channels of MCM-41 to form small $FePO_4$ clusters. The difference in the UV–vis spectra between the Rh–$FePO_4$/MCM-41 and the Rh/$FePO_4$/MCM-41 was not significant, however.

$H_2$-TPR profiles for these MCM-41-supported samples and $FePO_4$ are plotted in Fig. 12. The peak for the reduction of $FePO_4$ to $Fe_2P_2O_7$ was markedly shifted to a lower temperature (from 951 to 751 K) by the introduction of $FePO_4$ into MCM-41, confirming the formation of small $FePO_4$ clusters probably located inside the mesoporous channels [39,45]. The $H_2$-TPR profile for Rh–$FePO_4$/MCM-41 was obviously different from that for Rh/$FePO_4$/MCM-41. Two separate reduction peaks at 447 and 666 K were observed for Rh/$FePO_4$/MCM-41, and the quantitative calculation revealed that these two peaks corresponded to the reduction of $Rh^{3+}$ to $Rh^0$ and that of $FePO_4$ to $Fe_2P_2O_7$, respectively. The two reduction peaks moved to 490 and 595 K, respectively, and became overlapped for Rh–$FePO_4$/MCM-41. The high-temperature shift for $Rh^{3+}$ reduction and the low-temperature shift for $FePO_4$ reduction indicate that there are stronger interactions between $Rh^{3+}$ species and $FePO_4$ clusters in this sample. It is reasonable to speculate that there are more dual sites containing both $Rh^{3+}$ and $FePO_4$ in close proximity in the Rh–$FePO_4$/MCM-41 sample.

### *3.3. Catalyst requirements for methyl acetate formation and possible reaction mechanism*

As described in Section 3.1, the doping of rhodium to $FePO_4$ induced the formation of $CH_3COOCH_3$ during the conversion of $CH_4$ with $N_2O$ and CO. However, different preparation methods resulted in Rh-doped $FePO_4$ catalysts with different catalytic performances. The doping of rhodium to $FePO_4$ by the impregnation method markedly decreased the rate of $CH_3OH$ formation (Table 1). The con-

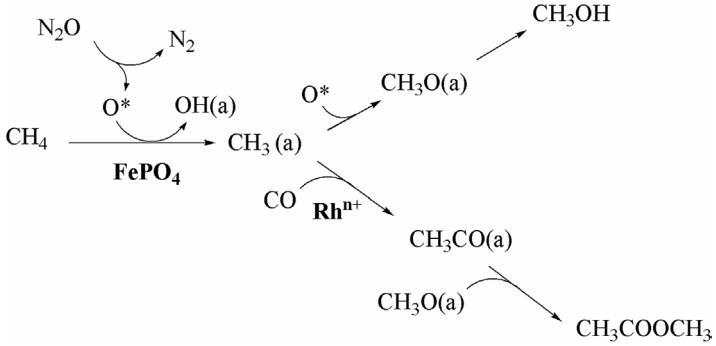


Scheme 1.

version of $N_2O$ was also decreased at the same time, suggesting that the activation of $N_2O$ to active oxygen species responsible for $CH_4$ conversion was suppressed. The characterizations for the $Rh/FePO_4$ series of samples indicated that Rh(III) species were mainly located on the surface of $FePO_4$ and might aggregate into small $Rh_2O_3$ clusters or particles at a high rhodium content. The covering of some iron sites by the Rh(III) species may be a reason for the decreases in the conversion of $N_2O$ and in the rate of $CH_3OH$ formation over this series of catalysts. On the other hand, as suggested by the characterizations with XRD, diffuse-reflectance UV–vis, and $H_2$-TPR, rhodium was probably incorporated into the lattice of $FePO_4$ and existed in the state of highly dispersed $Rh^{3+}$ in the $Rh–FePO_4$ series of samples prepared from the mixed aqueous solution. The decreases in the conversion of $N_2O$ and in the rate of $CH_3OH$ formation were not so significant after the introduction of rhodium to $FePO_4$ for this series of catalysts. Higher rates and TOFs for $CH_3COOCH_3$ formation were obtained over this series of catalysts. It is speculated that the higher dispersion of $Rh^{3+}$ into the lattice of $FePO_4$ may account for the higher catalytic performances of the $Rh–FePO_4$ series of catalysts. The higher dispersion of $Rh^{3+}$ in $FePO_4$ may cause the formation of a higher concentration of dual sites containing both $Rh^{3+}$ and $FePO_4$, which are probably responsible for $CH_3COOCH_3$ formation.

The support of Rh(III) species and $FePO_4$ by MCM-41 can drastically increase the rate and TOF for $CH_3COOCH_3$ formation. However, an appropriate preparation method is also required to obtain higher catalytic performances. Co-impregnation has been found to be a much better method for $CH_3COOCH_3$ formation than the two-step impregnation. $H_2$-TPR results strongly suggest that there are stronger interactions between Rh(III) species and $FePO_4$ in the $Rh–FePO_4/MCM$-41 sample prepared by co-impregnation. These results further support the conclusion that the dual sites containing Rh(III) species and $FePO_4$ in close proximity account for the conversion of $CH_4$ to $CH_3COOCH_3$ with $N_2O$ and CO.

On the basis of kinetic investigations, we propose that the formation of $CH_3COOCH_3$ probably proceeds via the mechanism shown in Scheme 1. It is known that the iron sites in $FePO_4$ [46,47] or in the ZSM-5 zeolite [48,49] can activate $N_2O$ forming active oxygen species, which are responsible for the conversion of $CH_4$ into $CH_3OH$ or $CH_3O$ species via $CH_3$ species. As described above, the covering of the surface of $FePO_4$ by Rh(III) species really decreased the conversion of $N_2O$ and the rate of $CH_3OH$ formation. To further examine the possibility that the iron site and the phosphate group are both necessary, the 0.11 wt% Rh/MCM-41 and 0.11 wt% Rh–3.4 wt% $FeO_x$/MCM-41 (Rh/Fe = 1:60) catalysts, prepared by the impregnation and co-impregnation methods, respectively, have been investigated for the conversion of $CH_4$ with $N_2O$ and CO. As shown in Table 4, no formation of $CH_3OH$ was observed over either catalyst.

Table 4
Comparisons of some catalysts for the conversion of $CH_4$ with $N_2O$ and CO[a]

| Catalyst[b] | $N_2O$ conversion (%) | Formation rate (μmol $g^{-1}$ $h^{-1}$) | | TOF for $CH_3COOCH_3$ ($h^{-1}$) |
|---|---|---|---|---|
| | | $CH_3OH$ | $CH_3COOCH_3$ | |
| 0.11% Rh–9.1% $FePO_4$/MCM-41 | 99 | 587 | 696 | 65.2 |
| 0.11% Rh/MCM-41 | ∼100 | 0 | 3.5 | 0.33 |
| 0.11% Rh–3.4% $FeO_x$/MCM-41 | ∼100 | 0 | 0 | 0 |
| 0.11% Rh–9.1% $FePO_4$/MCM-41[c] | ∼100 | 0 | 0 | 0 |
| 0.11% Rh–$FePO_4$ | 6.8 | 517 | 65.4 | 6.12 |
| 0.11% Rh–$FePO_4$[c] | 13.2 | 550 | 0 | 0 |
| 0.11% Rh–$FePO_4$[d] | 6.7 | 849 | 26.6 | 2.49 |

[a] Reaction conditions: catalyst, 0.2 g; temperature, 723 K; $P(CH_4) = 52.9$ kPa; $P(N_2O) = 16.5$ kPa; $P(CO) = 31.9$ kPa; total flow rate, 53.4 $cm^3$ $min^{-1}$.
[b] The number before % denotes the content in weight percentage in each sample.
[c] The catalyst was pre-reduced in a gas flow containing 5% $H_2$ and 95% Ar at 553 K for 0.5 h before reaction.
[d] The catalyst was pretreated in a gas flow containing 60% CO and 40% He at 723 K for 0.5 h before reaction.

A very small amount of $CH_3COOCH_3$ was formed over the 0.11 wt% Rh/MCM-41, but no such formation was observed over the 0.11 wt% Rh–3.4 wt% $FeO_x$/MCM-41. The 100% conversion of $N_2O$ over both catalysts suggests that the reaction between $N_2O$ and CO (reaction (6)) dominates. Thus both the iron site and the phosphate group play important roles in the activation of $N_2O$ for the selective conversion of $CH_4$ in our case.

The rhodium species are proposed to work for the carbonylation of the $CH_3$ intermediate to produce the adsorbed acetyl ($CH_3CO$) intermediate. To determine whether metallic rhodium ($Rh^0$) or rhodium cations account for the carbonylation, the effect of the pre-reduction on catalytic properties of the 0.11 wt% Rh–9.1 wt% $FePO_4$/MCM-41 and 0.11 wt% Rh–$FePO_4$ samples has been investigated. As shown in Table 4, although the change in $CH_3OH$ formation depended on the catalyst and the reductant ($H_2$ or CO) used, the formation of $CH_3COOCH_3$ was inhibited in all of the cases in which the pre-reduced catalysts were used. When $H_2$ was used as the reductant, no $CH_3COOCH_3$ could be observed over either catalyst, indicating that $Rh^0$ was inactive for the carbonylation. We have checked the oxidation state of rhodium by XPS for the 0.34 wt% Rh–$FePO_4$ catalyst after the reaction in $CH_4$, $N_2O$, and CO under the conditions shown in Table 1. The result reveals that the rhodium is still kept in the $Rh^{3+}$ state after the reaction (curve d in Fig. 4). Moreover, the supported $Rh^0$ has been reported to catalyze the reduction of $N_2O$ by CO [50], which is the most undesirable side reaction in this study. Thus it is likely that keeping the rhodium in a cationic state during the reaction is crucial for avoiding this side reaction and for the occurrence of the carbonylation.

Rhodium is known to be the active component for the carbonylation of $CH_3OH$ in the Monsanto process [51]. A Rh(I) complex, $[RhX_2(CO)_2]^-$ (X = halide), has been recognized as the active complex in this process. The Rh(I) complex is transformed into a Rh(III) complex, $[RhX_3(CH_3)(CO)_2]^-$, via the oxidative addition of $CH_3X$, and then an acetylrhodium complex is formed by the insertion of CO to Rh–$CH_3$ [52]. Over the Rh(III)-X zeolite, which is an effective heterogeneous catalyst for the carbonylation of $CH_3OH$, the formation of Rh(I) carbonyl intermediate, $Rh(I)(CO)_2$, has been suggested by XPS and IR studies [53]. This Rh(I) intermediate has also been proposed to interact with $CH_3I$, producing an acetylrhodium intermediate similar to that observed in the homogeneous case [53]. We speculate that a Rh(I) carbonyl intermediate may also be formed in our case during the reaction. As shown in Scheme 1, over our catalysts, the $CH_3$(a) species generated from the activation of $CH_4$ may migrate to the rhodium site coordinated by CO. Then the insertion of CO will result in the formation of an acetylrhodium intermediate. $CH_3COOCH_3$ must be formed by the reaction of the acetylrhodium intermediate with the $CH_3O$(a) species. Since the activation of $CH_4$ occurs on $FePO_4$ while the carbonylation takes place on rhodium cations, the presence of dual sites containing both rhodium cations and $FePO_4$ in close proximity is crucial for the formation of $CH_3COOCH_3$.

## 4. Conclusions

Two series of Rh-doped $FePO_4$ samples prepared by different methods show different catalytic properties for the conversion of methane to methyl acetate with $N_2O$ and CO. The Rh–$FePO_4$ series of samples prepared from the mixed aqueous solution exhibits a higher rate and TOF for methyl acetate formation than the Rh/$FePO_4$ series of samples prepared by the impregnation method. It has been clarified through detailed characterizations that Rh(III) species or $RhO_x$ clusters are mainly located on the surface of $FePO_4$ in the Rh/$FePO_4$ samples, whereas $Rh^{3+}$ cations are probably dispersed in the lattice of $FePO_4$ in the Rh–$FePO_4$ samples. The higher concentration of the dual sites containing both rhodium cations and $FePO_4$ in close proximity probably accounts for the better catalytic performances of the Rh–$FePO_4$ series of samples for methyl acetate formation. The support of rhodium species and $FePO_4$ by MCM-41 by the co-impregnation method greatly accelerates the conversion of methane to methyl acetate, whereas the two-step impregnation method cannot lead to effective catalysts. There probably are more dual sites of Rh(III) species and $FePO_4$ in close proximity in the MCM-41-supported catalysts prepared by the co-impregnation method. The highest rate and TOF for methyl acetate formation obtained in this study are ca. 0.7 mmol $g^{-1}$ $h^{-1}$ and 65 $h^{-1}$, respectively. A reaction mechanism for the conversion of methane to methyl acetate has been described through kinetic analysis.

## Acknowledgments

This work was supported by the National Natural Science Foundation of China (Nos. 20433030, 20021002, and 20273054), the Program for New Century Excellent Talents at the University of China (No. NCET-04-0602), the Creative Research Foundation for Young Scientists by Fujian Province of China (No. 2001J029), and the National Basic Research Program of China (No. 2003CB615803).

## References

[1] R. Pitchai, K. Klier, Catal. Rev. Sci. Eng. 28 (1986) 13.
[2] N.D. Parkyns, C.I. Warburton, J.D. Wilson, Catal. Today 18 (1993) 385.
[3] T.J. Hall, J.S.J. Hargreaves, G.J. Hutchings, R.W. Joyner, S.H. Taylor, Fuel Proc. Technol. 42 (1995) 151.
[4] R.H. Crabtree, Chem. Rev. 95 (1995) 987.
[5] A.E. Shilov, G.B. Shul'pin, Chem. Rev. 97 (1997) 2879.
[6] A. Sen, Acc. Chem. Res. 31 (1998) 550.
[7] J.A. Labinger, J.E. Bercaw, Nature 417 (2002) 507.
[8] J.H. Lunsford, Catal. Today 63 (2000) 183.
[9] K. Otsuka, Y. Wang, Appl. Catal. A 222 (2001) 145.

[10] K. Tabata, Y. Teng, T. Takemoto, E. Suzuki, M.A. Banares, M.A. Pena, J.L.G. Fierro, Catal. Rev. Sci. Eng. 44 (2001) 1.
[11] C. Jia, T. Kitamura, Y. Fujiwara, Acc. Chem. Res. 34 (2001) 633.
[12] F. Arena, A. Parmaliana, Acc. Chem. Res. 36 (2003) 867.
[13] Y. Wang, K. Otsuka, Catalysts & Catalysis (Shokubai) 46 (2004) 595.
[14] D. Wolf, Angew. Chem. Int. Ed. 37 (1998) 3351.
[15] R.A. Periana, D.J. Taube, E.R. Evitt, D.G. Loffer, P.R. Wentrcek, T. Masuda, Science 259 (1993) 340.
[16] R.A. Periana, D.J. Taube, S. Gamble, H. Taube, T. Satoh, H. Fujii, Science 280 (1998) 560.
[17] R.A. Periana, O. Mironov, D. Taube, G. Bhalla, C.J. Jones, Science 301 (2003) 814.
[18] S. Mukhopadhyay, M. Zerella, A.T. Bell, R.V. Srinivas, G.S. Smith, Chem. Commun. (2004) 472.
[19] M. Zerella, S. Mukhopadhyay, A.T. Bell, Chem. Commun. (2004) 1948.
[20] H. Hogeveen, J. Lukas, C.F. Roobeek, Chem. Commun. (1969) 920.
[21] A. Bagno, J. Bukala, G.A. Olah, J. Org. Chem. 55 (1990) 4284.
[22] M. Lin, A. Sen, Nature 368 (1994) 613.
[23] M. Lin, T.E. Hogan, A. Sen, J. Am. Chem. Soc. 118 (1996) 4574.
[24] G.V. Nizova, G. Süss-Fink, S. Stanislas, G.B. Shul'pin, Chem. Commun. (1998) 1885.
[25] Y. Taniguchi, T. Hayashida, H. Shibasaki, D. Piao, T. Kitamura, T. Yamaji, Y. Fujiwara, Org. Lett. 1 (1999) 557.
[26] M. Asadullah, T. Kitamura, Y. Fujiawara, Angew. Chem. Int. Ed. 39 (2000) 2475.
[27] P.M. Reis, J.A.L. Silva, A.F. Palavra, J.J.R.F. da Silva, T. Kitamura, Y. Fujiawara, A.J.L. Pombeiro, Angew. Chem. Int. Ed. 42 (2003) 821.
[28] E.M. Wilcox, G.W. Roberts, J.J. Spivey, Appl. Catal. A 226 (2002) 317.
[29] M. Golombok, T. Nijbacker, M. Raimondi, Ind. Eng. Chem. Res. 43 (2004) 6001.
[30] Z. Yang, J. Xue, S. Shen, H. Wang, Acta Phys.-Chim. Sin. 12 (1996) 741.
[31] W. Huang, K.-C. Xie, J.-P. Wang, Z.-H. Gao, L.-H. Yin, Q.-M. Zhu, J. Catal. 201 (2001) 100.
[32] E.M. Wilcox, G.W. Roberts, J.J. Spivey, Catal. Today 88 (2003) 83.
[33] N. Maeda, T. Miyao, S. Naito, Catal. Lett. 91 (2003) 175.
[34] Y. Li, C-J. Liu, B. Eliasson, Y. Wang, Energy Fuels 16 (2002) 864.
[35] Y. Wang, M. Katagiri, K. Otsuka, Chem. Commun. (1997) 1187.
[36] Y. Wang, K. Otsuka, J. Catal. 155 (1995) 256.
[37] Q. Zhang, Y. Wang, Y. Ohishi, T. Shishido, K. Takehira, J. Catal. 202 (2001) 308.
[38] Y. Wang, Q. Zhang, T. Shishido, K. Takehira, J. Catal. 209 (2002) 186.
[39] X. Wang, Y. Wang, Q. Tang, Q. Guo, Q. Zhang, H. Wan, J. Catal. 217 (2003) 457.
[40] A.M. Beale, G. Sankar, J. Mater. Chem. 12 (2002) 3064.
[41] R.S. Weber, J. Catal. 151 (1995) 470.
[42] M. Kawai, M. Uda, M. Ichikawa, J. Phys. Chem. 89 (1985) 1654.
[43] G. Fröhlich, W.M.H. Sachtler, J. Chem. Soc. Faraday Trans. 94 (1998) 1339.
[44] W.C. Conner Jr., J.L. Falconer, Chem. Rev. 95 (1995) 759.
[45] Y. Wang, X. Wang, Z. Su, Q. Gu, Q. Tang, Q. Zhang, H. Wan, Catal. Today 93–95 (2004) 155.
[46] Y. Wang, K. Otsuka, J. Chem. Soc. Faraday Trans. 91 (1995) 3953.
[47] Y. Wang, K. Otsuka, J. Catal. 171 (1997) 106.
[48] G.I. Panov, A.K. Uriarte, M.A. Rodkin, V.I. Sobolev, Catal. Today 41 (1998) 365.
[49] B.R. Wood, J.A. Reimer, A.T. Bell, M.T. Janicke, K.C. Ott, J. Catal. 225 (2004) 300.
[50] P. Granger, P. Malfoy, G. Leclercq, J. Catal. 223 (2004) 142.
[51] D. Forster, Adv. Organomet. Chem. 17 (1979) 255.
[52] D. Forster, J. Am. Chem. Soc. 98 (1976) 846.
[53] S.L.T. Andersson, M.S. Scurrell, J. Catal. 59 (1979) 340.